# Characterizing foam flow in fractures for enhanced oil recovery

AlQuaimi, B. I.; Rossen, W. R.

**DOI**
10.1016/j.petrol.2018.06.020

**Publication date**
2018

**Document Version**
Final published version

**Published in**
Journal of Petroleum Science and Engineering

Journal of Petroleum Science and Engineering 175 (2019) 1160–1168

Contents lists available at ScienceDirect

Journal of Petroleum Science and Engineering

journal homepage: www.elsevier.com/locate/petrol

# Characterizing foam flow in fractures for enhanced oil recovery

B.I. AlQuaimi[a,b,*], W.R. Rossen[a]

[a] Department of Geoscience and Engineering, Delft University of Technology, Netherlands
[b] Saudi Aramco, Dhahran, Saudi Arabia

ABSTRACT

Gas is used in displacing oil for enhanced oil recovery because of its high microscopic-displacement efficiency. However, the process at the reservoir scale suffers from poor sweep efficiency due to density and viscosity differences compared to in-situ fluids. Foam substantially increases the viscosity of injected gas and hence improves the sweep. Foam rheology in 3D geological porous media has been characterized both theoretically and experimentally. In contrast, the knowledge of foam flow in fractured porous media is far less complete. A companion paper (AlQuaimi and Rossen, 2017c), We focused on foam generation and propagation in a fully characterized model fracture. Here we focus on foam rheology in the same model fracture. This investigation is conducted by varying superficial velocities of gas and surfactant solution. We find in this model fracture the same two foam-flow regimes central to the understanding of foam in 3D porous media: a low-quality regime where pressure gradient is independent of liquid velocity and a high-quality regime where pressure gradient is independent of gas velocity. The transition between regimes is less abrupt than in 3D porous media. Our study directly relates flow regime to foam texture through observation of bubble size, bubble trapping and mobilization, and foam stability as functions of superficial velocities which allows comparison with our understanding of the mechanisms behind the two flow regimes in 3D porous media. Additionally, foam is shear-thinning in both regimes. However, the mechanisms thought to be behind the two flow regimes in 3D porous media do not appear in our model fracture. Foam is not at the limit of stability in the high-quality regime. Mobility in the high-quality regime, instead, reflects reduced and fluctuating foam generation at high foam quality. Moreover, bubble size is not fixed at approximately pore size, the mechanism thought to control the low-quality regime in 3D porous media. Instead, bubbles are much smaller than pores. Finally, for this model fracture, the investigation of vertical flow reaches the same findings as for horizontal flow, with somewhat lower pressure gradient.

## 1. Introduction

Underground reservoirs that include natural fractures impose additional challenges for enhanced oil recovery (EOR) projects. The challenges are encountered because of the presence of highly conductive fractures or fissures (Allan and Sun, 2003). Injected gas designed to recover un-displaced oil flow rapidly in the fractures, reducing the efficiency of the process. The gas has high microscopic-displacement efficiency. However, the process at the reservoir scale suffers from poor sweep efficiency (Cinar et al., 2007; Aryana and Kovscek, 2012; Worthen et al., 2015). Foam greatly reduces gas mobility and hence allows gas to encounter more oil (Fjelde et al., 2008; Haugen et al., 2014; Steinsbø et al., 2015). Numerous studies have characterized foam rheology in 3D geological porous media, both theoretically and experimentally, but far fewer for fractured porous media.

A companion paper (AlQuaimi and Rossen, 2017c), reviews previous research on foam generation in model fractures. Here we focus on the findings of those studies on foam rheology in fractures and the mechanisms behind it.

Kovscek et al. (1995) investigated nitrogen, water and aqueous foam flow through two transparent replicas of natural rough-walled rock fractures with hydraulic apertures of both roughly 30 μm and 100 μm. Radial-flow tests were done on these fractures, with a diameter of 12 cm. The total flow rate of nitrogen ranged from 1 to 100 standard $cm^3$/min, which is equivalent to 0.0014–0.147 m/s at the outer radius. They concluded that the rheology of foam in fractures is complicated. At gas fractional flows, i.e. foam qualities, above 0.97 the pressure drop was proportional to the liquid flow rate at a fixed gas flow rate. For gas fractional flows below approximately 0.9, the pressure drop was insensitive to the liquid flow rate. At intermediate gas fractional flow, the pressure drop decreased with increasing liquid flow rate. These results would be consistent with the two flow regimes identified in 3D porous media (Alvarez et al., 2001).

Buchgraber et al. (2012) experimentally investigated the behavior of pre-generated foam in fractures at various foam qualities and fluid velocities. The experiments were conducted in fractures etched on 2 × 5 cm silicon chips. The first experiment was done in smooth channels with apertures of 40 and 30 μm. The second experiment was conducted in a smooth slit with apertures of 20 and 40 μm arranged in a checkerboard pattern. The third experiment was done on a uniform-aperture channel with a rough face. The gas superficial velocity ranged from $7.23 \times 10^{-6}$- 0.0057 m/s and the liquid superficial velocity ranged from $2.89 \times 10^{-5}$– 0.0017 m/s. Low- and high-quality regimes were identified. These explained the low pressure gradient observed in

* Corresponding author. Department of Geoscience and Engineering, Delft University of Technology, Netherlands.
*E-mail address:* bander.quaimi@aramco.com (B.I. AlQuaimi).

https://doi.org/10.1016/j.petrol.2018.06.020
Received 9 August 2017; Received in revised form 3 June 2018; Accepted 6 June 2018
Available online 15 June 2018
0920-4105/ 

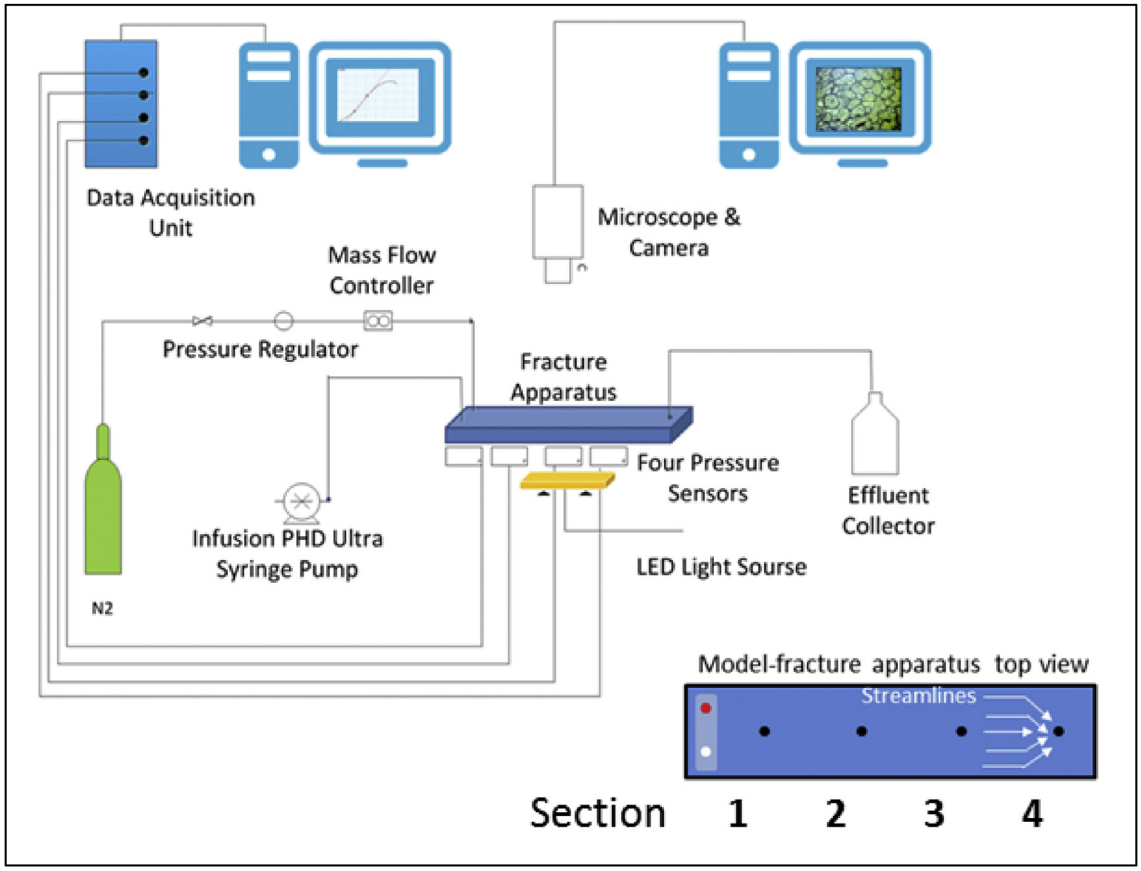


**Fig. 1.** Schematic of the experimental setup.

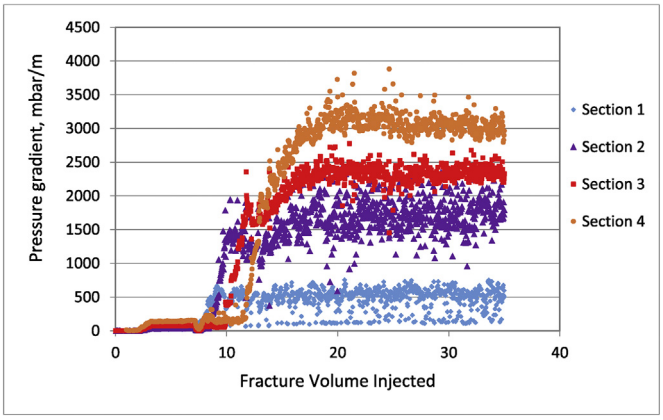


**Fig. 2.** Pressure gradient during a foam-injection test at a foam quality of 37%.

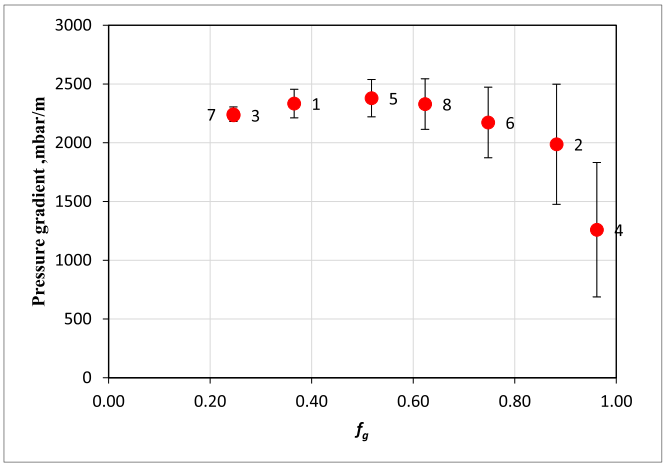


**Fig. 3.** Foam-quality scan (pressure-gradient as a function of foam quality $f_g$) at total superficial velocity $u_t = 0.0021$ m/s.

the high-quality regime as the result of coalescence of foam.

Fernø et al. (2016) reported a study of foam flow behavior in a fractured rock slab 31.2 cm long. The total superficial velocities used were 0.0003, 0.001, 0.0017 and 0.0028 m/s. Increased pressure gradient was observed at increased foam quality, for a given total flow rate. At high foam quality the pressure gradient suddenly dropped. They explained this sudden decrease as the result of the dry conditions leading to foam coalescence.

In this study, we investigate the rheology of in-situ-generated foam in a well-characterized transparent model fracture. We compare the behavior of foam using four total superficial velocities (0.0011, 0.0021, 0.0030, and 0.0049 m/s) and foam qualities ranging from 23 to 97%. We measure the pressure difference across four sections along the fracture and capture images to explain the foam behavior.

## 2. Fracture physical model

The fracture apparatus and the model fracture were used previously to study foam generation and propagation in fractures (AlQuaimi and Rossen, 2017c). The 40 × 10 cm model fracture consists of a roughened plate that represents fracture-wall roughness and a top plate that is smooth, to allow direct observation of the flow. The gap between the top plate and the rough surface represents the fracture aperture. The following details are relevant to the practicalities of this study of foam rheology. The two glass plates are glued together at the edges using Araldite®2014, which is a two-component epoxy adhesive that has a tensile strength of 26 MPa at 23 °C. The 4 mm-thick roughened plate

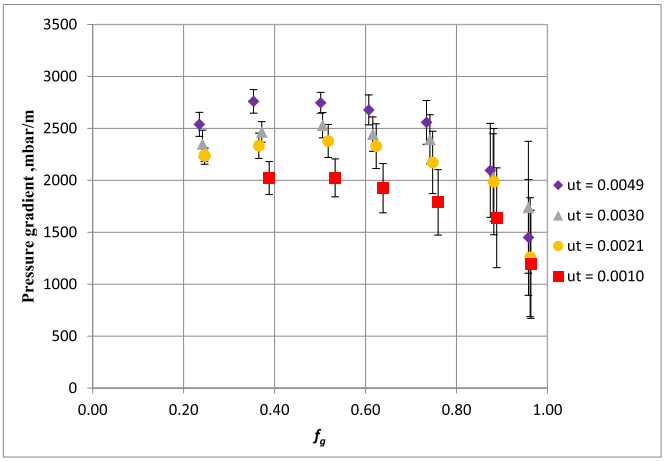


**Fig. 4.** Foam-quality scan at different total superficial velocities (m/s).

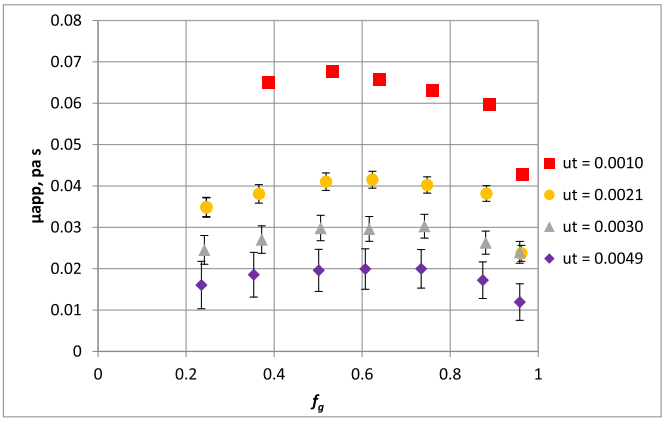


**Fig. 5.** Foam apparent viscosity as a function of foam quality at different total superficial velocities.

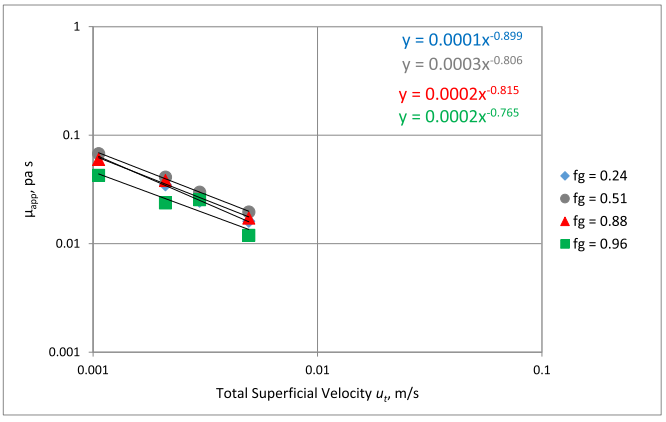


**Fig. 6.** Foam apparent viscosity as a function of total superficial velocity at fixed foam quality.

was strengthened by attaching a 15 mm-thick glass plate using ultraviolet light and DELO®-Photobond® glue (DELO, Windach, Germany). The thickness of the top glass plate is 15 mm as well. The thickness of the glass was estimated based on solid-mechanics calculations to prevent any significant glass deflection during the flow. This is also checked using a Probe Indicator (2 μm resolution) during the experiment. Four pressure ports are equally spaced over a length of 36 cm; the last port is also the fluid outlet (Fig. 1). The fracture is mounted in a frame that could slide 50 cm in the X and Y directions to allow for microscopic observation of the flow in the whole 40 × 10 cm fracture. Further details can be found in (AlQuaimi and Rossen, 2017c).

The model fracture has been characterized in terms of average aperture and variability and correlation length of aperture, allowing its representation as a 2D porous medium with pore throats and bodies. Using this characterization we previously combined the capillary number-residual saturation curve for a wide range of model fractures into a single relationship (AlQuaimi and Rossen, 2017a, 2017b). The roughened glass used to make the model fracture in this study has a regular, square pattern in its roughness, as illustrated in Figs. 9 and 11 below. A full description of the model fracture geometry can be found in (AlQuaimi and Rossen, 2017c). This study is part of a larger effort to examine foam behavior in a wide variety of model fractures and relate the behavior to dimensionless geometrical factors that can be applied to natural fractures in the field.

## 3. Experimental procedure

The same experimental setup described in (AlQuaimi and Rossen, 2017c) is used here. The pressure gradient in the first section is affected by the entry region and the last section by converging flow towards the outlet. We therefore selected the third section on which to base our analysis of the pressure behavior in this paper. We averaged the pressure gradient over the period of stabilization for each foam quality. The hydraulic aperture of this model fracture is 66 μm.

The foam experiment starts by co-injecting a solution of 1.0 wt.% sodium C14-16 olefin sulfonate and nitrogen into the fully water-saturated fracture. The two fluids enter the model fracture at the entry region and flow into the fracture. In-situ foam generation is observed as discussed in (AlQuaimi and Rossen, 2017c). The pressure gradient is recorded until stabilization is reached. Fig. 2 shows the evolution of the pressure gradient as the water initially present is displaced and foam is generated in our experiment. The test was conducted at a foam quality ($f_g$) of 37% and total superficial velocity of 0.0021 m/s. Oscillation in $|\nabla P|$ is observed in this test, and larger oscillation is evident at higher $f_g$. The injected gas volume is corrected to the pressure at the middle of the fracture. We performed foam-quality scans at fixed total superficial velocity ($u_t$). The pressure-gradient data were acquired in a non-uniform sequence to avoid any hysteresis that may occur in the case of sequential increase or decrease in $f_g$ (Fig. 3). The data points have numbers which indicate the sequence in which they were acquired. The error bars in the plot indicate the standard deviation of the measurement. Additionally, point 3 at $f_g = 0.25$ was repeated after displacing all the foam and starting the experiment again with only water in the fracture. This gives extra confidence in the measurement and the procedure followed to acquire the data. The oscillation in $|\nabla P|$ reflects fluctuation in foam generation, as discussed below.

## 4. Experimental results

We tested four total superficial velocities $u_t$, 0.0010, 0.0021, 0.0030, and 0.0049 m/s (Fig. 4). As the velocity increases the pressure gradient increases; however, the increase is not proportional to $u_t$. At a total superficial velocity of 0.0010 m/s, the lowest $f_g$ that can be achieved within the limits of our gas mass-flow meter/mass-flow controller is 0.38. We used Eq. (1) to estimate foam apparent viscosity in these four tests (Fig. 5).

$$\mu_{app} = \frac{1}{12}\frac{|\nabla P| w d_H^3}{Q} \quad (1)$$

where $|\nabla P|$ is pressure gradient, $w$ is the width perpendicular to flow, $d_H$ is the hydraulic aperture, and $Q$ is volumetric flow rate. The largest mobility reduction is achieved at a velocity of 0.0010 m/s. A mobility reduction by a factor of 67 relative to that of water in single-phase flow is estimated at $f_g$ of 0.53. If we estimate mobility reduction to the gas

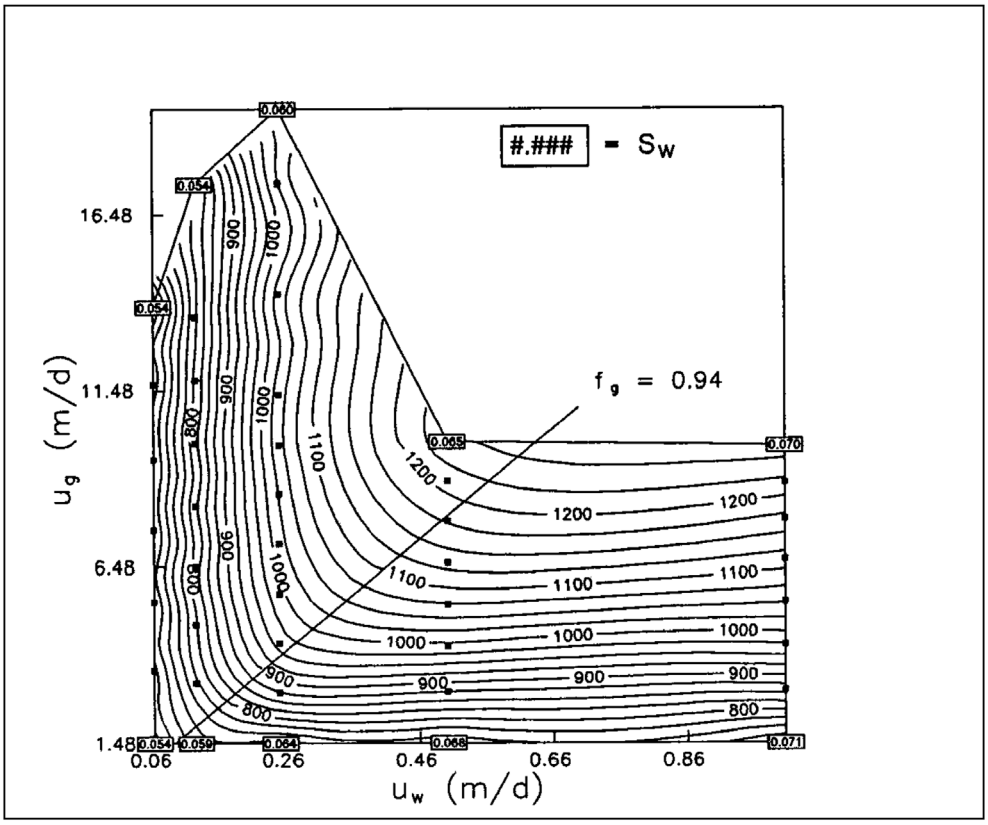


**Fig. 7.** Effects of gas and liquid velocity on steady-state foam flow. This figure is from Osterloh and Jante (1992).

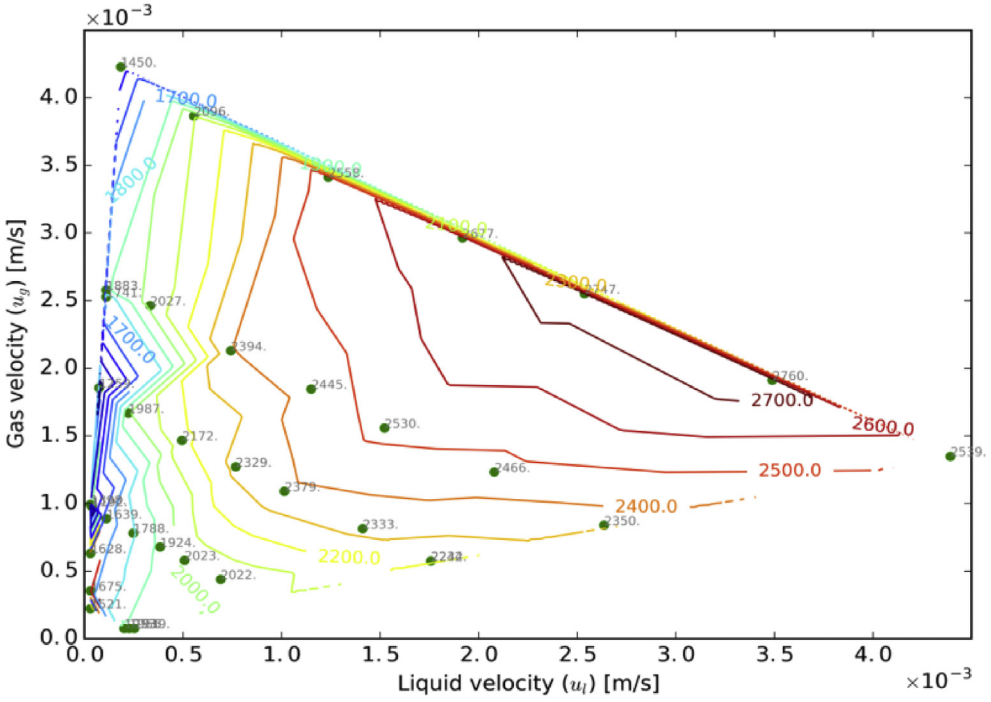


**Fig. 8.** Pressure gradient (mbar/m) as a function of superficial velocities of gas and liquid; existence of two flow regimes in fracture. Contor lines shift smoothly from horizontal to vertical, i. e. between low quality to high quality.

phase alone, this estimate would be much larger. Fig. 5 indicates that foam is shear-thinning and Fig. 6 shows that foam apparent viscosity is shear-thinning with respect to superficial velocity, with average exponent of about (−0.82). Represented as a power law fluid (Bird, 2002), this corresponds to a power law exponent n = 0.18. Previous studies (Kovscek et al., 1995; Fernø et al., 2016) also found shear-thinning rheology in the model of a real fracture.

Central to the understanding of flow in 3D porous media is the existence of two distinct foam-flow regimes, corresponding to high foam quality and low foam quality (Osterloh and Jante, 1992; Alvarez

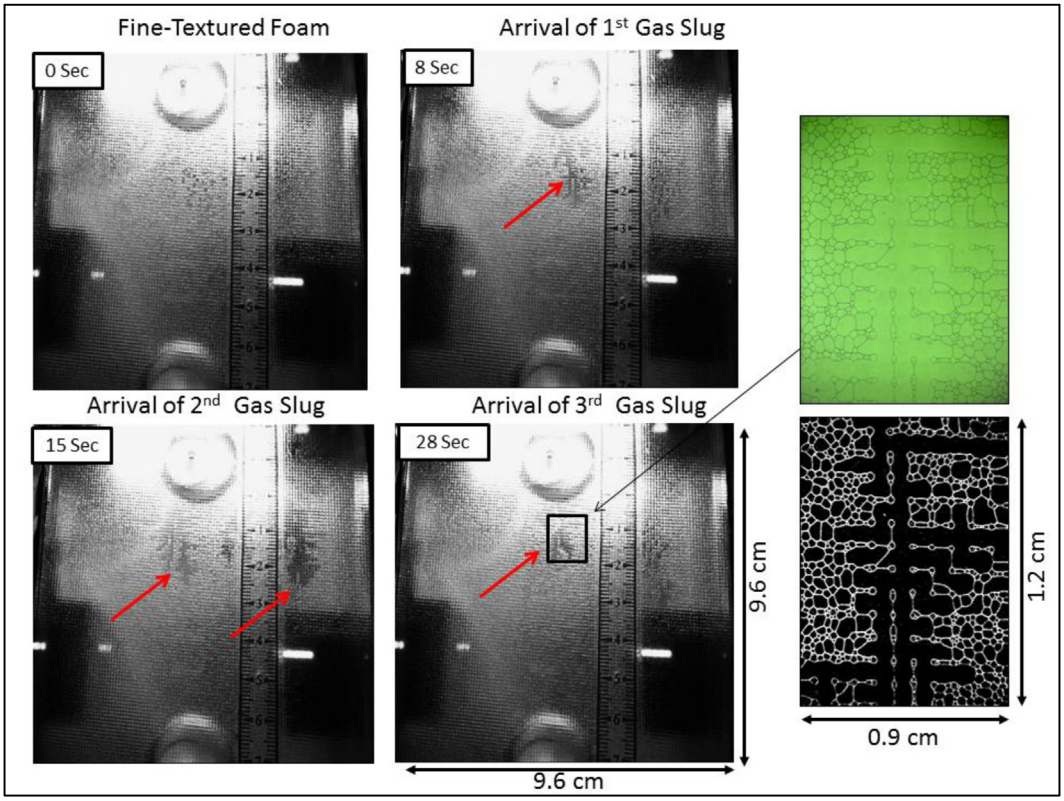


**Fig. 9.** Time-lapse images of reduced and fluctuating foam generation. The enlarged images at right show a gas slug. (This binary image is the processed version: black is gas and white is foam films (lamellae).) Total superficial velocity $u_t = 0.0030$ m/s and $f_g = 0.90$. Flow is from the top of the image to the bottom; the fracture itself is horizontal.

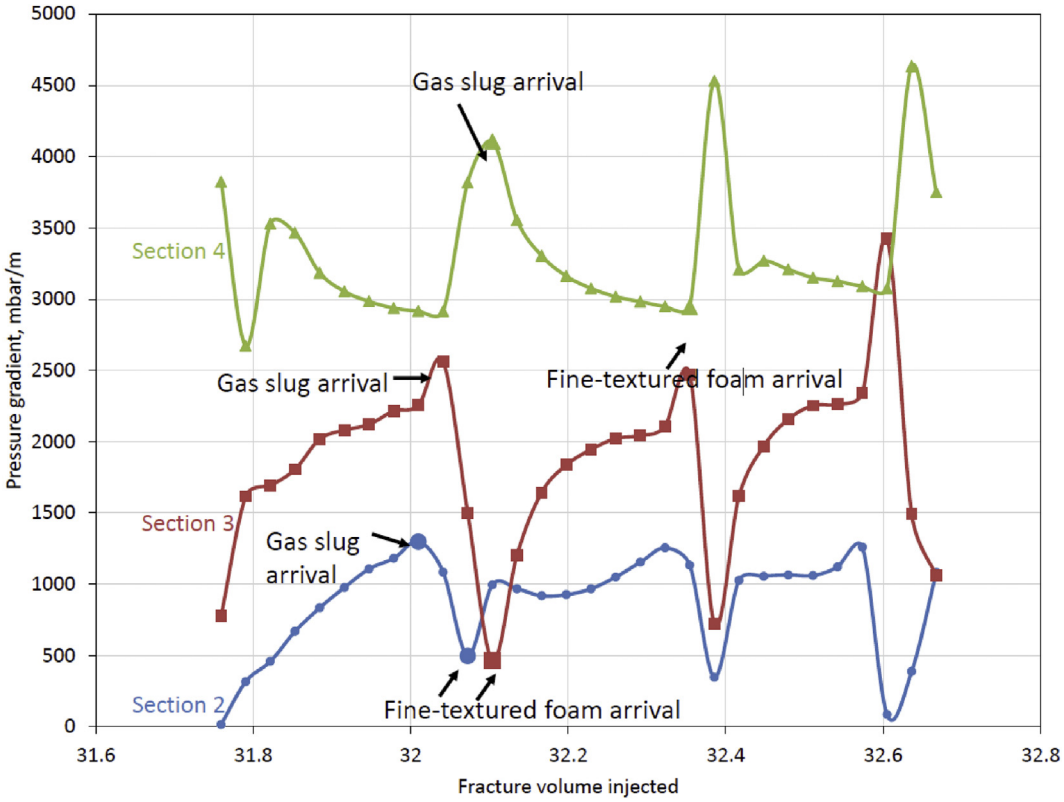


**Fig. 10.** Pressure gradient in three sections of the model fracture during coinjection of gas and liquid $u_t = 0.0010$ m/s and $f_g = 0.88$. The pressure gradient increases as fine-textured foam behind the gas slug reaches the section. The curves connect the points to guide the reader's eye.

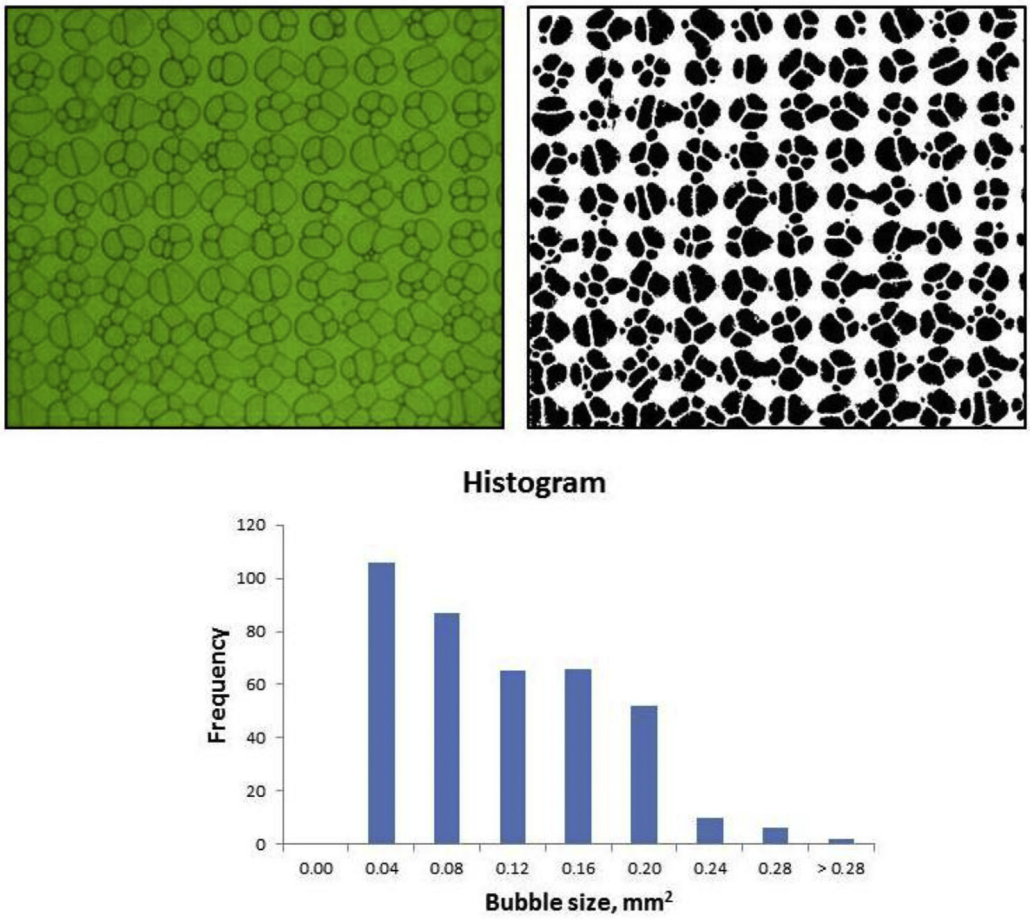


**Fig. 11.** Image (0.97 × 0.82 cm) taken at low foam quality $u_t$ = 0.0010 m/s and $f_g$ = 0.38 and the binary version of it (top). Black is gas and white is water. The histogram shows the bubble-size distribution.

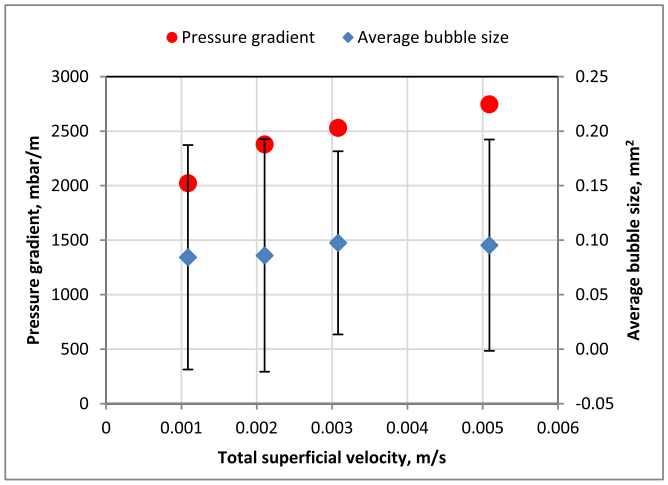


**Fig. 12.** Pressure gradient and average bubble size vs. $u_t$ at $f_g$ = 0.51.

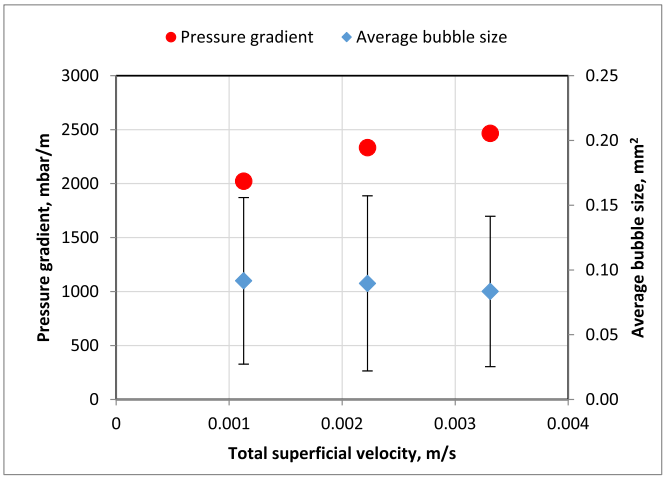


**Fig. 13.** Pressure gradient and average bubble size vs. $u_t$ at $f_g$ = 0.38.

et al., 2001). Fig. 7 is from is from Osterloh and Jante (1992). Pressure gradient is independent of liquid velocity in the low-quality regime and independent of gas velocity in the high-quality regime. We investigated the existence of these two flow regimes in our model fracture. The pressure-gradient data were plotted using a Julia (open source programming language: julialang.org) script, to construct a contour plot from the data. The plot shows the existence of two flow regimes in the fracture similar to those in 3D porous media (Fig. 8). Fig. 8 reveals a broader transition; pressure contor lines shift smoothly from horizontal to vertical, between the two qualities, than usually seen in 3D porous media (e.g. Fig. 7). The explanation for pressure-gradient behavior in the high-quality regime in 3D porous media is that foam collapse at the limiting capillary pressure ($P_C$*) controls bubble size and therefore gas mobility (Khatib et al., 1988). In the low-quality regime, bubble size is thought to be unchanging at approximately pore size, and pressure gradient depends on porous medium and surface tension, but not on the ability of the surfactant to stabilize foam (Rossen and Wang, 1999). The

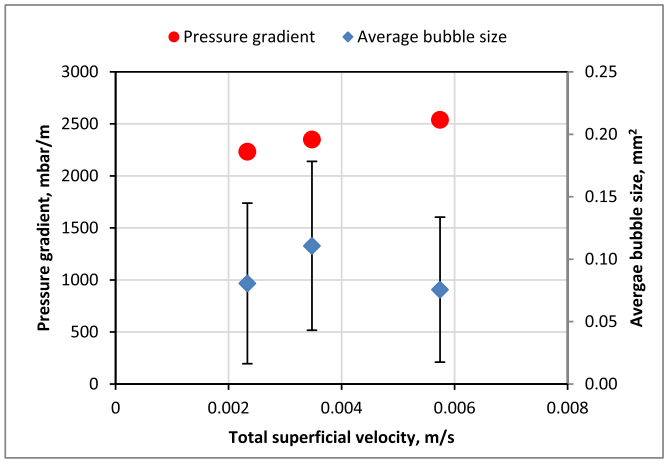


**Fig. 14.** Pressure gradient and average bubble size vs. $u_t$ at $f_g = 0.24$.

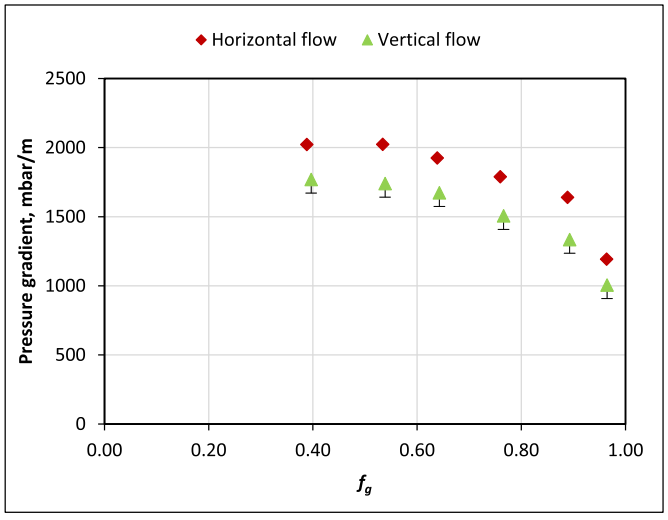


**Fig. 15.** Comparison between pressure gradient in vertical flow and horizontal flow at $u_t = 0.0010$ m/s. The vertical lines on the data for vertical flow represent the magnitude of the gravitational potential for the liquid in these experiments.

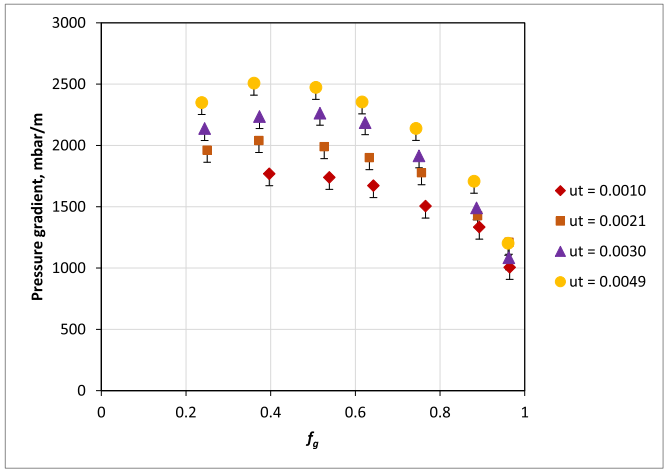


**Fig. 16.** Foam-quality scan at different total superficial velocities (m/s) in upward vertical flow. The error bars represent the magnitude of the effect of gravity on the liquid flow potential, i.e., the difference from the values measured in horizontal flow.

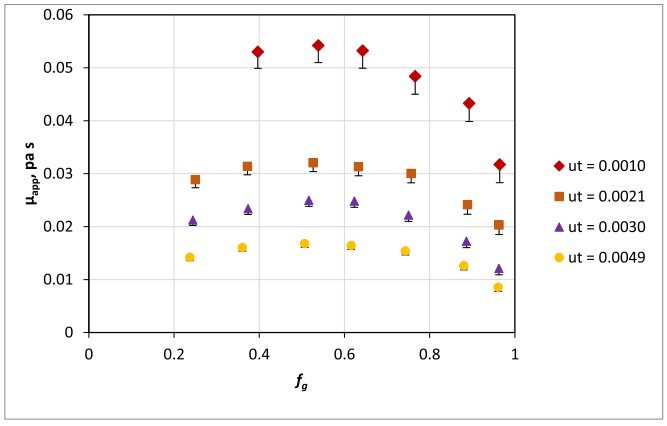


**Fig. 17.** Foam apparent viscosity at different total superficial velocities during upward vertical flow. The error bars represent the effect of gravity on the liquid flow potential.

transition between regimes is sensitive to both the nature of the porous medium and ability of the surfactant to stabilize foam (Alvarez et al., 2001).

In our model fracture, we observe different phenomena controlling the two flow regimes from those believed to operate in 3D porous media. Several images were captured and analyzed using ImageJ, an image-processing and analysis software. We followed systematic steps in the analysis of the images using image thresholding to detect the boundaries of the foam bubbles and determine bubble sizes. At high foam quality, we see reduced and fluctuating foam generation, but steady foam generation at low quality. At high foam quality, fine-textured foam is generated and propagates, followed by a slug of gas that is refined as it propagates (Fig. 9). This causes the pressure response to fluctuate and hence reduces time-average foam apparent viscosity. Fig. 9 shows the time interval between the individual gas slugs at $u_t = 0.0030$ m/s and $f_g = 0.90$. The length of the gas slug and its velocity increase as $f_g$ increases. The pressure-gradient data correlate well with this observation. At steady state, we tracked the pressure behavior as the slug propagates downstream using the pressure sensors spaced over the entire length of the fracture at $u_t = 0.0030$ m/s and $f_g = 0.96$ (Fig. 10). The pressure decreases sequentially as the slug arrives at the downstream section, and increases as the fine-textured foam behind it reaches the section. At low foam quality, foam is generated mainly by capillary snap-off and the average bubble size remains constant at a size less than pore size (0.50 mm$^2$) (Fig. 11). (Kovscek et al., 1995) reported behavior consistent with the high- and low-quality flow regimes in a model fracture (Buchgraber et al., 2012) report observing the two flow regimes in a microfluidic device and ascribe the high-quality regime to foam coalescence at high foam quality.

Three low foam qualities $f_g$, 0.24, 0.38 and 0.51, are used to investigate the foam texture at different $u_t$. The pressure gradient, as shown in Fig. 4, increases as $u_t$ increases at a fixed $f_g$. However, we find that for these values of $u_t$ the average bubble size does not change greatly at fixed $f_g$ (Figs. 12–14). It is thought that average bubble size does not change in the low-quality foam regime in 3D porous media (Rossen and Wang, 1999; Alvarez et al., 2001). Bubbles are thought to be as large as pores in that regime. The near-invariance of bubble size in Figs. 12–14 is consistent with these findings, but bubbles are smaller than pores (0.50 mm$^2$). It is possible that bubble size reflects a characteristic size for snap-off in the throats rather than the pore-body size. Pore throats in this model are 5–10 times as wide across as the aperture, a slit-shaped geometry that favors snap-off (Rossen, 1996). The error bar on the average bubble size represents the standard deviation of bubble-size distribution.

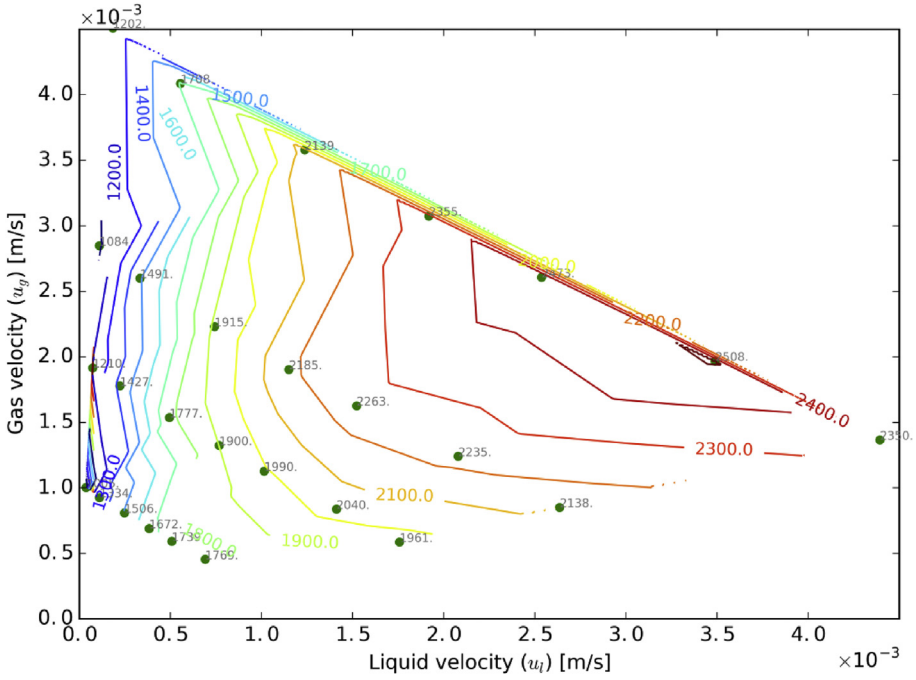


**Fig. 18.** Pressure gradient (mbar/m) as a function of superficial velocities of gas and liquid in upward vertical flow; existence of two flow regimes in the fractures.

## 5. Vertical flow experiment

We modified the experimental setup to study the effect of gravity on foam flow. The model fracture was oriented vertically such that gas and surfactant solutions are injected from the bottom. The other experimental conditions were held constant. We conducted a foam-quality scan at $u_t = 0.0010$ m/s (Fig. 15). The comparison between vertical flow with horizontal flow shows a somewhat lower pressure gradient during vertical flow. The difference is much greater than 100 mbar per meter, the difference between potential gradients for gas and liquid flow in gravity. The same trends observed in horizontal flow were observed also in vertical flow: Bubble size was roughly constant in the low-quality regime, and intermittent foam generation was prevalent in the high-quality regime.

We performed four foam-quality scans with four total superficial velocities $u_t$. The tested velocities are 0.0010, 0.0021, 0.0030, and 0.0049 m/s (Fig. 16). Similarly, we used Eq. (1) to estimate foam apparent viscosity in these four tests (Fig. 17). The largest mobility reduction is achieved in these tests at a velocity of 0.0010 m/s.

The pressure-gradient data were plotted to construct a contour plot, which shows again the existence of two flow regimes during vertical flow (Fig. 18). The observed behavior during vertical flow shows the same flow characteristics discussed above for horizontal flow (Fig. 8).

## 6. Summary and conclusions

The following conclusions can be drawn from our experimental investigation of foam rheology in a model fracture:

- The pressure gradient increased with increasing total superficial velocity of foam injection, but the increase in pressure gradient was not proportional to superficial velocity. Instead it reflects shear-thinning behavior, with an average exponent of approximately (−0.82) (apparent power-law-fluid exponent n = 0.18).
- The pressure-gradient data for in-situ generated foam reveals the existence of two foam-flow regimes, i.e. high- and low-quality regimes, as seen in 3D porous media.
- These two foam-flow regimes were observed during horizontal flow and vertical flow. Somewhat lower pressure gradient was recorded in vertical flow, however.
- In our experiments, the high-quality regime is evidently the result of reduced and fluctuating foam generation, not foam collapse at the limiting capillary pressure. The pressure-gradient data correlates well with the propagation of gas slugs downstream and hence confirms this finding of fluctuating foam generation at high $f_g$.
- For three low foam qualities in horizontal flow, the images at different superficial velocities show no significant change in average bubble size with superficial velocity, but the bubbles are smaller than pores. It is possible that the bubble size reflects a characteristic size for snap-off in the throats.

## Acknowledgment

The authors acknowledge Saudi Aramco for providing the scholarship for Mr. AlQuaimi, and also the generous support provided by the sponsors of the Joint Industry Project on Foam for Enhanced Oil Recovery at Delft University of Technology.

## References

Allan, J., Sun, S.Q., 2003. Controls on recovery factor in fractured reservoirs: lessons learned from 100 fractured fields. In: Paper Presented at the SPE Annual Technical Conference and Exhibition. Denver, Colorado, U.S.A. 5 – 8 October 2003, SPE-84590-MS.

AlQuaimi, B.I., Rossen, W.R., 2017a. Capillary desaturation curve for residual nonwetting phase in natural fractures. SPE J. https://doi.org/10.2118/189448-PA.

AlQuaimi, B.I., Rossen, W.R., 2017b. New capillary number definition for displacement of residual nonwetting phase in natural fractures. Geophys. Res. Lett. 44 (11), 5368–5373. https://doi.org/10.1002/2017GL073211.

AlQuaimi, B.I., Rossen, W.R., 2017c. Study of foam generation and propagation in a fully characterized physical-model fracture. In: Submitted to the Journal of Petroleum Science and Engineering.

Alvarez, J.M., Rivas, H.J., Rossen, W.R., 2001. Unified model for steady-state foam behavior at high and low foam qualities. SPE J. https://doi.org/10.2118/74141-PA.

Aryana, S.A., Kovscek, A.R., 2012. Experiments and analysis of drainage displacement processes relevant to carbon dioxide injection. Phys. Rev. 86 (6), 066310.

Bird, R.B., 2002. Transport phenomena. Appl. Mech. Rev. 55 (1), R1–R4.

Buchgraber, M., Castanier, L.M., Kovscek, A.R., 2012. Microvisual investigation of foam flow in ideal fractures: role of fracture aperture and surface roughness. In: Paper Presented at the SPE Annual Technical Conference and Exhibition.

Cinar, Y., Riaz, A., Tchelepi, H.A., 2007. Experimental study of CO2 injection into saline formations. In: Paper Presented at the SPE Annual Technical Conference and Exhibition.

Fernø, M.A., Gauteplass, J., Pancharoen, M., Haugen, Å., Graue, A., Kovscek, A.R., Hirasaki, G., 2016. Experimental study of foam generation, sweep efficiency, and flow in a fracture network. SPE J. 21 (4), 1140. https://doi.org/10.2118/170840-PA.

Fjelde, I., Zuta, J., Duyilemi, O.V., 2008. Oil recovery from matrix during CO2-foam flooding of fractured carbonate oil reservoirs. In: Paper Presented at the Europec/EAGE Conference and Exhibition, 9–12 June 2008, Rome, Italy.

Haugen, Å., Mani, N., Svenningsen, S., Brattekås, B., Graue, A., Ersland, G., Fernø, M.A., 2014. Miscible and immiscible foam injection for mobility control and EOR in fractured oil-wet carbonate rocks. Transport Porous Media 104 (1), 109–131.

Khatib, Z., Hirasaki, G., Falls, A., 1988. Effects of capillary pressure on coalescence and phase mobilities in foams flowing through porous media. SPE Reservoir Eng. 3 (03), 919–926.

Kovscek, A., Tretheway, D., Persoff, P., Radke, C., 1995. Foam flow through a transparent rough-walled rock fracture. J. Petrol. Sci. Eng. 13 (2), 75–86.

Osterloh, W., Jante, M., 1992. Effects of gas and liquid velocity on steady-state foam flow at high temperature. In: Paper Presented at the SPE/DOE Enhanced Oil Recovery Symposium.

Rossen, W.R., 1996. Foams in enhanced oil recovery. Surfactant Sci. Ser. 413–464.

Rossen, W.R., Wang, M.W., 1999. Modeling foams for acid diversion. SPE J. 4 (2), 92–100. https://doi.org/10.2118/56396-PA.

Steinsbø, M., Brattekås, B., Ersland, G., Bø, K., Opdal, I., Tunli, R., et al., 2015. Foam as mobility control for integrated CO2-EOR in fractured carbonates. In: Paper Presented at the IOR 2015–18th European Symposium on Improved Oil Recovery, Dresden, Germany 14-16 April 2015.

Worthen, A., Taghavy, A., Aroonsri, A., Kim, I., Johnston, K., Huh, C., et al., 2015. Multi-scale evaluation of nanoparticle-stabilized CO 2-in-Water foams: from the benchtop to the field. In: Paper Presented at the SPE Annual Technical Conference and Exhibition.